Nrf2 Redirects Glucose and Glutamine into Anabolic Pathways in Metabolic Reprogramming

Yoichiro Mitsuishi,[1,2,6] Keiko Taguchi,[1,6] Yukie Kawatani,[1] Tatsuhiro Shibata,[4] Toshihiro Nukiwa,[2] Hiroyuki Aburatani,[5] Masayuki Yamamoto,[1,*] and Hozumi Motohashi[3,*]

[1]Department of Medical Biochemistry
[2]Department of Respiratory Medicine
[3]Center for Radioisotope Sciences
Tohoku University Graduate School of Medicine, 2-1 Seiryo-machi, Aoba-ku, Sendai, Miyagi, 980-8575, Japan
[4]Division of Cancer Genomics, Center for Medical Genomics, National Cancer Center Research Institute, 5-1-1, Tsukiji, Chuo-ku, Tokyo, 104-0045, Japan
[5]Research Center for Advanced Science and Technology, The University of Tokyo, 4-6-1, Komaba, Meguro-ku, Tokyo, 153-8904, Japan
[6]These authors contributed equally to this work
*Correspondence: masiyamamoto@med.tohoku.ac.jp (M.Y.), hozumim@med.tohoku.ac.jp (H.M.)
DOI 10.1016/j.ccr.2012.05.016

SUMMARY

Cancer cells consume large quantities of nutrients and maintain high levels of anabolism. Recent studies revealed that various oncogenic pathways are involved in modulation of metabolism. Nrf2, a key regulator for the maintenance of redox homeostasis, has been shown to contribute to malignant phenotypes of cancers including aggressive proliferation. However, the mechanisms with which Nrf2 accelerates proliferation are not fully understood. Here, we show that Nrf2 redirects glucose and glutamine into anabolic pathways, especially under the sustained activation of PI3K-Akt signaling. The active PI3K-Akt pathway augments the nuclear accumulation of Nrf2 and enables Nrf2 to promote metabolic activities that support cell proliferation in addition to enhancing cytoprotection. The functional expansion of Nrf2 reinforces the metabolic reprogramming triggered by proliferative signals.

INTRODUCTION

Metabolic activities in proliferating cells are fundamentally different from those in quiescent cells (DeBerardinis et al., 2008). Quiescent cells invest large amounts of energy in the maintenance of functional and morphological integrity against extrinsic and intrinsic insults, including oxidative stress. In contrast, proliferating cells take up abundant nutrients, including glucose and glutamine, and shunt their metabolites into anabolic pathways. The signals that promote cell proliferation direct the reprogramming of metabolic activities, which pushes quiescent cells into proliferative states. Recent studies have revealed that oncogenic pathways involving oncogenes and tumor suppressor genes, such as c-Myc, p53, and PI3K-Akt, directly promote the uptake and metabolism of glucose and glutamine, resulting in metabolic features that are unique to proliferating cells (Kroemer and Pouyssegur, 2008; Tong et al., 2009; Dang, 2010).

The pentose phosphate pathway (PPP) generates ribose 5-phosphate (R5P), a critical substrate for the nucleotide synthesis, and NADPH as reducing equivalents. Although the PPP is a well-established metabolic pathway, a direct regulator that activates the PPP during metabolic reprogramming has yet to be identified. One of the p53 targets, TIGAR, inhibits glycolysis and diverts the carbon flux into the PPP, resulting in the passive promotion of the PPP activity (Bensaad et al., 2006). However, because glycolysis is often facilitated in proliferating cells, alternative mechanisms that actively promote the PPP are expected to be involved.

Significance

Nrf2 is an inducible transcription activator for cytoprotection from xenobiotic and oxidative stresses. Increasing attention has been paid to the role of Nrf2 in cancer cells because the constitutive stabilization of NRF2 has been observed in many human cancers that have poor prognoses. Recent studies revealed that antioxidant and detoxification activities carried out by Nrf2 confer growth advantages on cancer cells. In this study, we show that Nrf2 directly or indirectly facilitates the metabolic pathways that enhance cell proliferation in the presence of active PI3K-Akt signaling. Thus, Nrf2 contributes to cancer development by modulating metabolism in addition to enhancing cellular stress response. This study expands upon current knowledge regarding the role of Nrf2 in the malignant evolution of cancers.

Nrf2 is a master transcriptional activator of cytoprotective genes. It activates transcription in response to electrophiles and reactive oxygen species (ROS) (Itoh et al., 1997; Uruno and Motohashi, 2011). Under normal conditions, Nrf2 is constantly ubiquitinated by Keap1 and degraded by the proteasome. Exposure to the stimuli inactivates Keap1 and stabilizes Nrf2. Nrf2 then translocates into the nucleus, binds to the antioxidant response element (ARE) and activates the transcription of many cytoprotective genes that encode detoxifying enzymes and antioxidant proteins. The induction of these genes confers resistance against xenobiotic and oxidative stresses. Recently, the constitutive stabilization of NRF2 was found in various human cancers (Singh et al., 2006; Shibata et al., 2008; Wang et al., 2008; Kim et al., 2010; Solis et al., 2010; Zhang et al., 2010). Cancers with high NRF2 levels are associated with poor prognosis (Shibata et al., 2008; Solis et al., 2010) not only because of the chemo- and radio-resistance but also the aggressive proliferation (Singh et al., 2008; Zhang et al., 2010). The molecular mechanisms that allow Nrf2 to promote cell proliferation have not yet been fully elucidated. To clarify how Nrf2 contributes to cell proliferation, we explored Nrf2 target genes in cancer cells. Hypothesizing that Nrf2 plays distinct roles in proliferating cells and quiescent cells, we attempted to identify a signal that modifies the Nrf2 function.

RESULTS

Nrf2 Activates Genes Involved in the PPP, De Novo Nucleotide Synthesis, and NADPH Production

NRF2 knockdown repressed the proliferation of cancer cell lines with constitutive NRF2 accumulation (A549, H2126, LK2 and EBC1 cells) (Figure 1A), suggesting that NRF2 accelerates the proliferation of these cells. Knockdown efficiency was monitored by the reduced expression of NAD(P)H:quinone oxidoreductase 1 (*NQO1*), one of the typical target genes of NRF2 (Figure 1B; Figure S1A available online).

To identify the target genes of NRF2 responsible for cell proliferation, we performed microarray analysis in A549 cells treated with *NRF2* siRNA or control siRNA. A549 is a lung cancer cell line in which NRF2 is constitutively stabilized due to a somatic mutation in the *KEAP1* gene (Taguchi et al., 2008) and the hypermethylation of the *KEAP1* promoter (Wang et al., 2008). We used three independent *NRF2* siRNAs and selected genes whose expression levels were reduced to less than 66.7% of that of the control sample by all three siRNAs to minimize off-target effects (Table S1). In addition to the typical target genes of NRF2 encoding detoxifying enzymes and antioxidant proteins (cytoprotective genes), genes whose products are involved in the PPP (glucose-6-phosphate dehydrogenase [*G6PD*], phosphogluconate dehydrogenase [*PGD*], transketolase [*TKT*], and transaldolase 1 [*TALDO1*]) and de novo nucleotide synthesis (phosphoribosyl pyrophosphate amidotransferase [*PPAT*] and methylenetetrahydrofolate dehydrogenase 2 [*MTHFD2*]) were decreased by the *NRF2* knockdown (Figure 1B). Genes encoding enzymes for NADPH synthesis (malic enzyme 1 [*ME1*] and isocitrate dehydrogenase 1 [*IDH1*]) were also decreased (Figure 1B). The *NRF2* knockdown did not affect the expression levels of four unrelated genes (*MDM2*, *CREBBP*, *EGFR*, and *ERBB2*) or the abundance of the ribosomal RNA primary transcript (pre-rRNA) (Figure 1B). These results indicate that the genes involved in the metabolism (metabolic genes) were specifically repressed by the *NRF2* knockdown and exclude the possibility that cell activities were generally impaired in *NRF2*-knockdown cells. We also confirmed the reduction of the enzyme proteins encoded by these genes in the *NRF2*-knockdown cells (Figure 1C). A time-course of the gene expression was consistent with the blunted increase in cell number (Figure S1B and Figure 1A).

We then performed global mapping of NRF2 binding sites in A549 cells using ChIP-seq analysis (to be published elsewhere). By integrating the results of the ChIP-seq and microarray analyses, we found that NRF2 directly activates *G6PD*, *PGD*, *TKT*, *TALDO1*, *ME1*, and *IDH1* through well-conserved AREs (Figures 1D and S1C). The ChIP-seq results were validated for each locus using quantitative polymerase chain reaction (PCR) (Figure 1E). The expression of these genes depended on NRF2 in three other cell lines with constitutively stabilized NRF2 (Figure S1A). Although the peaks in the *PPAT* and *MTHFD2* loci from the ChIP-seq analysis were not validated by quantitative PCR (data not shown), the abundance of *PPAT* and *MTHFD2* mRNAs was similarly decreased by *NRF2* knockdown in these cell lines (Figure S1A).

Nrf2 Promotes Purine Nucleotide Synthesis and Glutamine Metabolism

To elucidate the contribution of NRF2 to cellular metabolic activities, we performed metabolomic profiling using capillary electrophoresis mass spectrometry (CE-MS) in A549 cells treated with *NRF2* siRNA or control siRNA (Figure 2). Consistent with our finding that NRF2 activates the expression of enzymes for PPP and nucleotide synthesis (Figure 2A), *NRF2* knockdown significantly increased the levels of glycolytic intermediates, such as G6P, F6P, DHAP, pyruvate, and lactate (Figure 2B). The effect was more obvious at 48 hr after siRNA introduction than at 24 hr (Figure 2B; Tables S2 and S3). PRPP and IMP, the first product of the purine nucleotide synthesis, were decreased whereas the PPP intermediates (i.e., 6-PG, Ru5P, R5P and S7P) were increased (Figure 2C). These results were validated by a tracer study using [U-^{13}C$_6$] glucose (Figure 2D; Table S4). Importantly, 100% of IMP detected in the tracer study was [^{13}C$_5$] IMP, suggesting that the ribose ring (C$_5$) of IMP is all derived from glucose in A549 cells (Table S4). Thus, the decrease in IMP in the *NRF2*-knockdown cells indicates that NRF2 is required for the efficient purine nucleotide synthesis from glucose. We did not detect a significant contribution of NRF2 to the pyrimidine nucleotide synthesis.

To exclude the effect of the salvage pathway of the nucleotide synthesis, we performed a tracer study with [U-^{13}C$_6$] glucose using dialyzed fetal bovine serum (FBS) to remove purine bases from the medium (Figure S2; Table S5). In the *NRF2*-knockdown cells, [^{13}C$_5$] IMP and [^{13}C$_5$] ADP significantly decreased while metabolites in the PPP, glycolysis, TCA cycle, and serine synthesis pathway tended to increase, suggesting that the overall distribution of the glucose-derived ^{13}C was shifted away from the purine nucleotide synthesis. These results demonstrated that the steps from R5P to IMP via PRPP (the post-R5P steps) were delayed and that the PPP intermediates stagnated in the *NRF2*-knockdown cells.
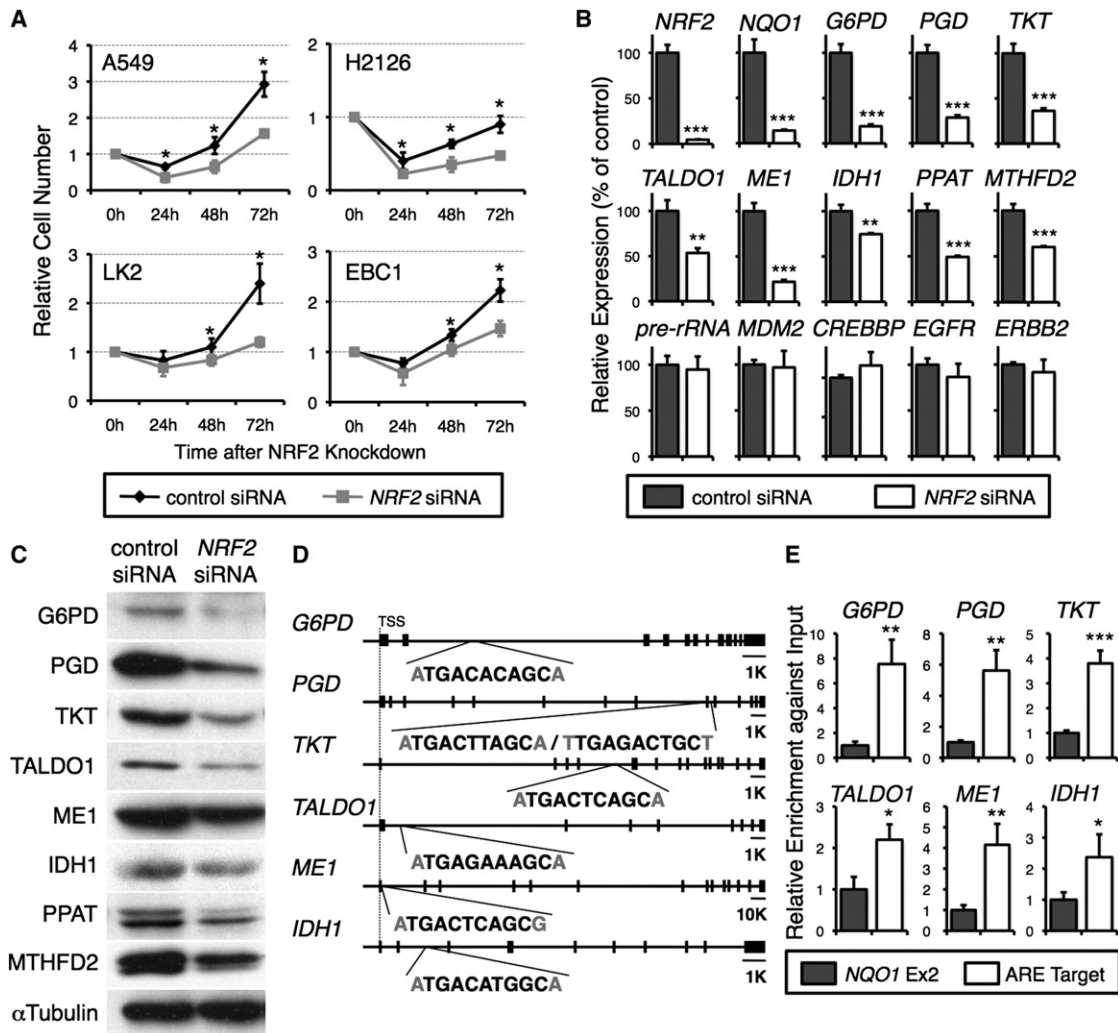
Figure 1. NRF2 Activates Genes Involved in the PPP, Nucleotide Synthesis, and NADPH Production

(A) Effects of *NRF2* knockdown on cell proliferation in cancer cell lines with the constitutive stabilization of NRF2. Cells were transfected with siRNA targeting *NRF2* (*NRF2* siRNA) or scrambled control siRNA (control siRNA). Initial cell numbers were set to 1.

(B) Effects of *NRF2* knockdown on gene expression in A549 cells. The mRNA expression was analyzed at 24 hr after the siRNA transfection. Each panel shows one representative result from three independent experiments. Average values and SDs were calculated from triplicate samples. Average values for cells treated with the control siRNA were set to 100. See also Table S1, Figures S1A and S1B.

(C) Immunoblot detection of the PPP enzymes and other metabolic enzymes in A549 cells. Cells were analyzed at 48 hr after the siRNA transfection. αTubulin was detected as a loading control.

(D) Position and sequence of AREs within each target locus. TSS, transcription start site. Scale bars indicate 1 kbp (1K) or 10 kbp (10K). See also Figure S1C.

(E) Relative enrichment against the input of each locus. The second exon of the *NQO1* gene (*NQO1* Ex2) was used as a negative control locus, whose enrichment was set to 1. One representative result from three independent experiments is shown. Average values and SDs were calculated from triplicate samples.

$*p < 0.05$; $**p < 0.01$; $***p < 0.001$ (A, B, and E).

One unexpected finding was a marked increase in glutamine and glutamate in the *NRF2*-knockdown cells (Figure 2F), which was suggestive of the critical contribution of Nrf2 to glutamine metabolism. The tracer study using [U-^{13}C$_5$] glutamine demonstrated the primary distribution of carbons derived from glutamine (Table S6). The two major directions of the metabolite flux were toward the glutathione synthesis and TCA cycle (Figure 2E). Remarkably, *NRF2* knockdown affected glutathione synthesis, decreasing the levels of ^{13}C-labeled GSH and GSSG (Figure 2G). This result is consistent with previous reports demonstrating that

Nrf2 activates both genes encoding the catalytic and regulatory subunits of gamma-glutamyl-cysteinyl-ligase (GCL), a rate-limiting enzyme of glutathione synthesis (Lu, 2009). Indeed, the knockdown of *KEAP1* and *NRF2* in HaCaT cells increased and decreased glutathione, respectively (MacLeod et al., 2009), indicating that Nrf2 plays an important role in glutathione synthesis. Another notable result of *NRF2* knockdown was an increase in [U-^{13}C$_4$] malate and a decrease in [U-^{13}C$_3$] lactate (Figure 2G), suggesting that lactate production from glutamine is inhibited. This result likely reflects the reduced activity of ME1 (Figures
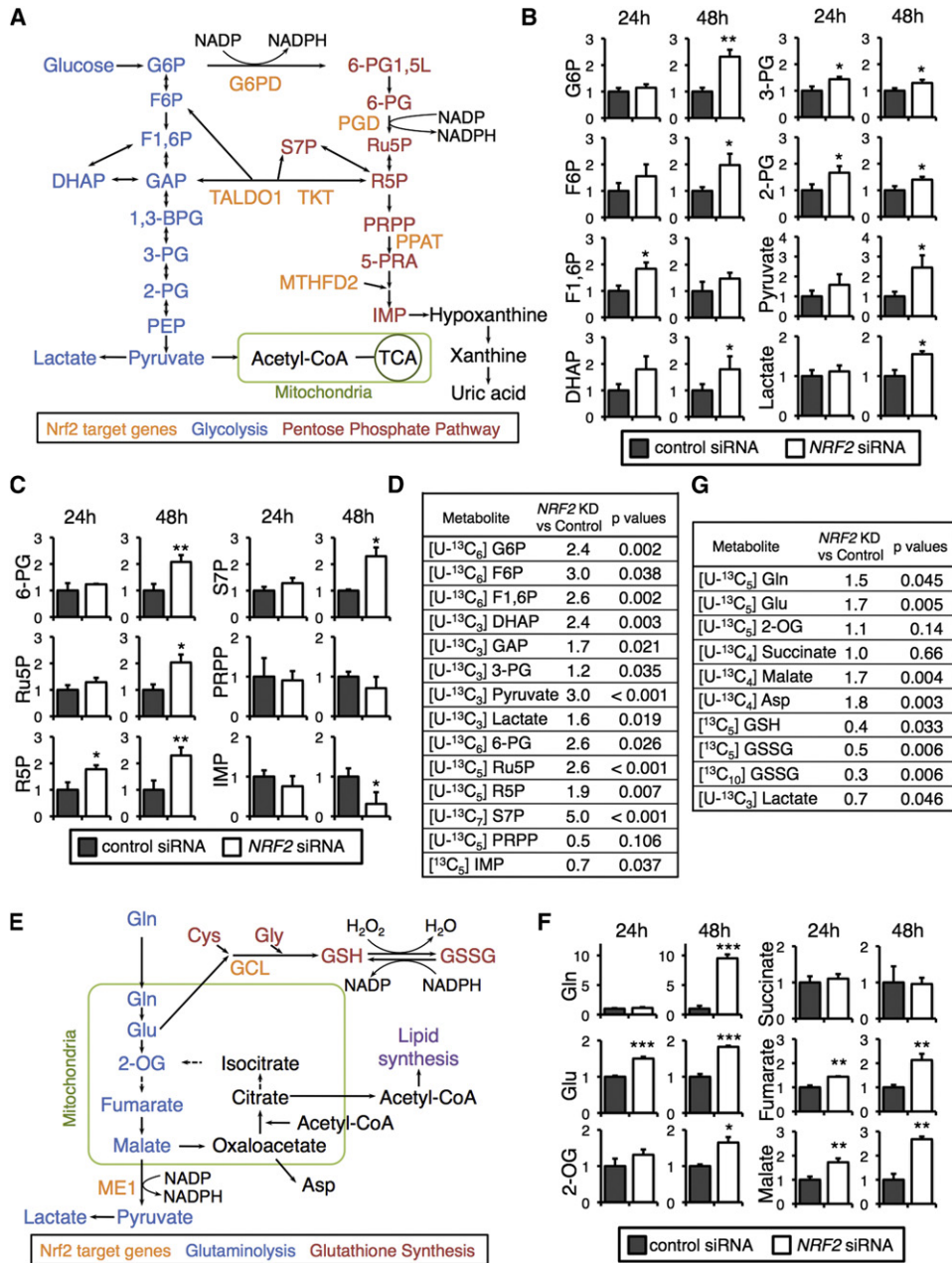
Figure 2. *NRF2* Knockdown Alters Glucose and Glutamine Metabolism in A549 Cells

(A) Metabolic enzymes regulated by NRF2 in glucose metabolism.

(B and C) Quantification of metabolic intermediates in glycolysis (B) and the PPP and purine nucleotide synthesis (C). Metabolite concentrations were quantified at 24 and 48 hr after the transfection of siRNAs. See also Tables S2 and S3.

(D) Tracer study using [U-^{13}C$_6$] glucose. A549 cells transfected with control siRNA or *NRF2* siRNA were incubated with [U-^{13}C$_6$] glucose for 1 hr and analyzed. Ratios of isotopomer concentrations in *NRF2*-knockdown (KD) samples versus control samples are shown. See also Tables S4 and S5 and Figure S2.

(E) Metabolic enzymes regulated by NRF2 in glutamine metabolism.

(F) Quantification of metabolic intermediates in glutathione synthesis and glutaminolysis. Metabolite concentrations were quantified at 24 and 48 hr after the transfection of siRNAs. See also Tables S2 and S3.

(G) Tracer study using [U-^{13}C$_5$] glutamine. A549 cells transfected with control siRNA or *NRF2* siRNA were incubated with [U-^{13}C$_5$] glutamine for 6 hr and analyzed. Ratios of isotopomer concentrations in *NRF2* KD samples versus control samples are shown. See also Table S6.

All samples were analyzed in triplicate. Error bars indicate SDs. *$p < 0.05$; **$p < 0.01$; ***$p < 0.001$ (B, C and F).

1,3-BPG, 1,3-bisphosphoglycerate; 2-OG, 2-oxoglutarate; 2-PG, 2-phosphoglycerate; 3-PG, 3-phosphoglycerate; 6-PG, 6-phosphogluconate; 6-PG1,5L, 6-phosphoglucono-1,5-lactone; 5-PRA, β-5-phosphoribosylamine; DHAP, dihydroxyacetone phosphate; F1,6P, fructose 1,6-bis-phosphate; F6P, fructose 6-phosphate; G6P, glucose 6-phosphate; GSSG, glutathione (oxidized); GSH, glutathione (reduced); GAP, glyceraldehyde 3-phosphate; IMP, inosine 5′-monophosphate; PEP, phosphoenolpyruvate; PRPP, phosphoribosyl pyrophosphate; R5P, ribose 5-phosphate; Ru5P, ribulose 5-phosphate; S7P, sedo-heptulose 7-phosphate.
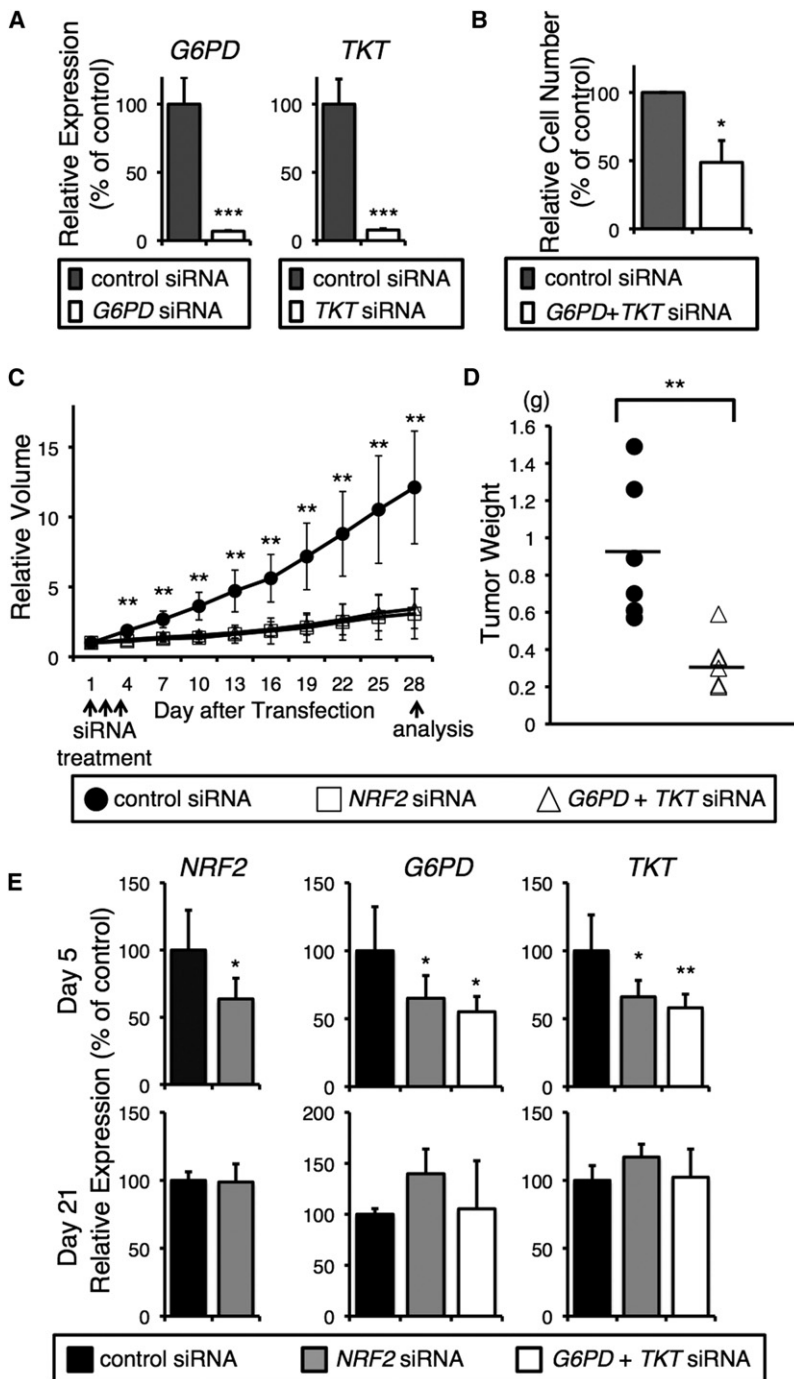
Figure 3. Functional Contribution of the PPP Enzymes to Cell Proliferation In Vitro and In Vivo

(A) Knockdown efficiencies of *G6PD* and *TKT* in A549 cells were examined by quantitative RT-PCR. Average values for cells treated with the control siRNA were set to 100.

(B) Effect of simultaneous knockdown of *G6PD* and *TKT* on cell proliferation. Relative cell numbers are shown. Cells were counted at 72 hr after transfection.

(C) Effect of simultaneous knockdown of *G6PD* and *TKT* on tumor growth in vivo. Mice transplanted with A549 cells were treated with control siRNA (n = 6), *NRF2* siRNA (n = 5), or *G6PD+TKT* siRNA (n = 6).

(D) Tumor weight on day 28 after the first siRNA treatment.

(E) mRNA expression of siRNA targets (*NRF2*, *G6PD*, and *TKT*) in tumors. The tumors were injected with control siRNA (n = 6 for day 5; n = 3 for day 21), *NRF2* siRNA (n = 6 for day 5; n = 3 for day 21), or *G6PD+TKT* siRNA (n = 5 for day 5; n = 3 for day 21) and processed for RNA purification at 5 or 21 days after the initial injection.

Average values and SDs were calculated from triplicate samples. Average values for cells treated with control siRNA were set to 100. *p < 0.05; **p < 0.01; ***p < 0.001 (A-E).

metabolite analysis, we separately evaluated the significance of the PPP for Nrf2-dependent proliferation. We examined the necessity of the PPP activity in NRF2-overexpressing cells by knocking down *G6PD* and *TKT*, which are involved in the oxidative and non-oxidative arms of the PPP, respectively (Figure 3). We used A549 cells in which NRF2 is abundantly expressed. The simultaneous knockdown of *G6PD* and *TKT* significantly repressed cell number increase after 72 hr of transfection (Figures 3A and 3B). The knockdown effect on tumor growth in vivo was examined in a xenograft experiment. Four weeks after A549 cells were transplanted into nude mice, the siRNA was injected into the tumor. Tumor growth was dramatically repressed by the injection of *NRF2* siRNA (Figure 3C). A previous study reported the therapeutic efficacy of the local injection of *NRF2* siRNA in a xenograft experiment (Singh et al., 2008), which was reproducible in our system. We further examined the efficacy of the double knockdown of *G6PD* and *TKT*. The simultaneous injection of siRNAs against *G6PD* and *TKT* was also effective for the inhibition of tumor growth (Figure 3C). The average tumor weight was significantly reduced by the double knockdown compared with the control samples (Figure 3D). Thus, the highly expressed NRF2 in A549 cells was insufficient to overcome the inhibitory effect on cell proliferation resulting from the *G6PD* and *TKT* knockdown. These data are consistent with a model in which G6PD and TKT are requisite downstream targets for NRF2 to support A549 cell proliferation.

The siRNA treatment of the tumor reduced the expression of the respective gene by approximately 40%–50% on day 5 (Figure 3E, upper panels), whereas no difference was detected on day 21 (Figure 3E, lower panels). These results suggest that
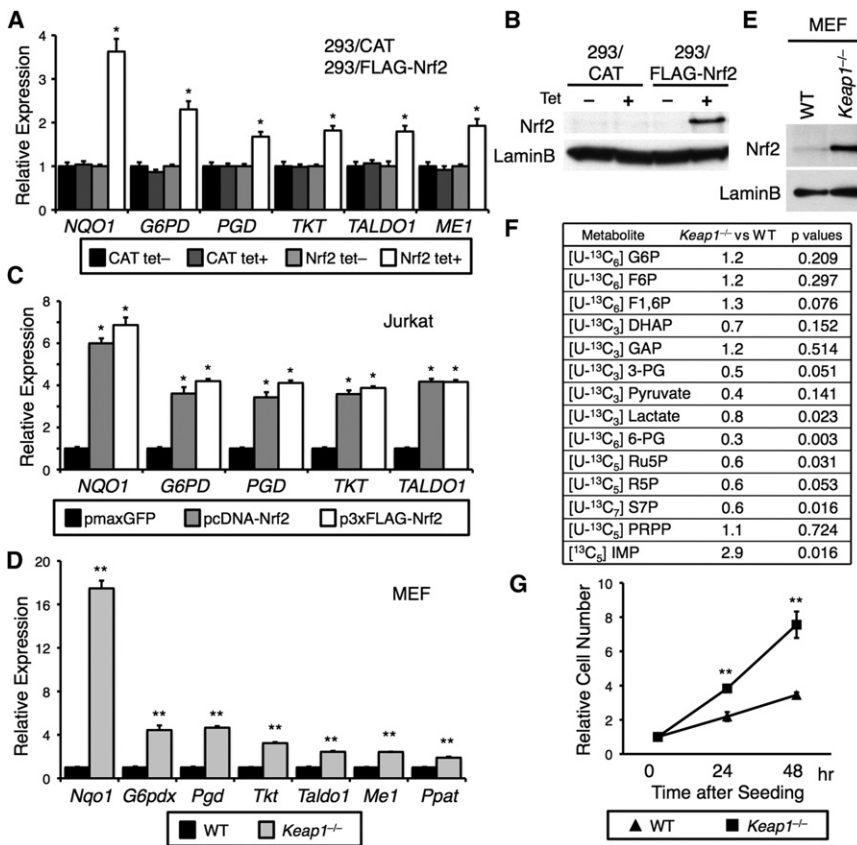
1B and 1C), which catalyzes the oxidative decarboxylation of malate and the production of NADPH. Indeed, the enzymatic activity of ME1 has been suggested to be responsible for glutaminolysis (DeBerardinis et al., 2007). Nrf2 thus facilitates glutaminolysis by activating ME1.

Nrf2 Requires the PPP Enzymes to Accelerate Tumor Growth

Since the inhibitory effect of the *NRF2* knockdown on the post-R5P steps seemed to dominate over that on the PPP in the

Figure 4. Effects of Nrf2 Overexpression in Cultured Cells

(A) Gene expression in 293/CAT and 293/FLAG-Nrf2 cells. Cells were treated with or without 1 μg/ml tetracycline for 24 hr. Average values for each cell without tetracycline were set to 1.

(B) Immunoblot analysis of Nrf2 in nuclear fractions of 293/CAT and 293/FLAG-Nrf2 cells. LaminB was detected as a loading control. Cells were treated with or without 1 μg/ml tetracycline for 24 hr.

(C) Gene expression in Jurkat cells transfected with pmaxGFP, pcDNA3-mNrf2 and p3xFLAG-Nrf2. Cells were harvested at 24 hr after the transfection. Average values for cells transfected with pmaxGFP were set to 1.

(D) Gene expression in WT and $Keap1^{-/-}$ MEFs. Average values for the WT MEFs were set to 1.

(E) Immunoblot analysis of Nrf2 in WT and $Keap1^{-/-}$ MEFs. LaminB was detected as a loading control.

(F) Tracer study using [U-^{13}C$_6$] glucose. WT and $Keap1^{-/-}$ MEFs were cultured with dialyzed FBS and incubated with [U-^{13}C$_6$] glucose for 1 hr. Ratios of isotopomer concentrations in $Keap1^{-/-}$ MEFs versus WT MEFs are shown. All samples were analyzed in triplicate. See also Table S7 and Figure S3.

(G) Cell proliferation of WT and $Keap1^{-/-}$ MEFs. Initial cell numbers were set to 1.

Average values and SDs were calculated from triplicate samples. *p < 0.01; **p < 0.001 (A, C, D and G).

the suppression of NRF2 activity or the PPP activity for a limited period sufficiently delayed tumor outgrowth and had a prolonged effect on tumor size.

Increased Expression of Nrf2 Alters Metabolic Activities and Enhances Proliferation in Cultured Cells

We next examined the effect of the increased Nrf2 on gene expression. 293/FLAG-Nrf2 and 293/CAT are stable cell lines that inducibly express FLAG-tagged Nrf2 and chloramphenicol acetyltransferase (CAT), respectively. After the induction with tetracycline, *NQO1*, one of the cytoprotective genes, and the metabolic genes were elevated in 293/FLAG-Nrf2 cells but not in 293/CAT cells (Figure 4A). The nuclear accumulation of Nrf2 was confirmed in 293/FLAG-Nrf2 cells treated with tetracycline (Figure 4B). When Nrf2 was overexpressed in Jurkat cells, in which Nrf2-mediated antioxidant response was augmented due to a frame-shift mutation in the *PTEN* gene (Sakamoto et al., 2009), *NQO1* and the metabolic genes were upregulated with the exception of ME1, whose expression was not detected in Jurkat cells (Figure 4C). We then examined the effect of the forced stabilization of endogenous Nrf2 by adopting $Keap1^{-/-}$ mouse embryonic fibroblasts (MEFs). $Keap1^{-/-}$ MEFs displayed abundant nuclear accumulation of Nrf2 and higher expression of the metabolic genes than wild-type (WT) MEFs (Figures 4D and 4E). Thus, Nrf2 activates the metabolic genes when it is highly expressed in cultured cells.

To examine the effect of Nrf2 increase on the nucleotide synthesis, $Keap1^{-/-}$ and WT MEFs were subjected to the tracer study using [U-^{13}C$_6$] glucose and dialyzed FBS. In $Keap1^{-/-}$ MEFs, [^{13}C$_5$] IMP, [^{13}C$_5$] AMP, and [^{13}C$_5$] ATP significantly increased while metabolites in the PPP, glycolysis, TCA cycle and serine synthesis pathway tended to decrease, suggesting that the overall distribution of the glucose-derived ^{13}C was shifted toward the purine nucleotide synthesis (Figures 4F and S3; Table S7). The post-R5P steps were facilitated in $Keap1^{-/-}$ MEFs, which was just opposite to the effect of *NRF2*-knockdown in A549 cells.

We then examined the effect of Nrf2 accumulation on cell proliferation. The cell number increase was much faster in $Keap1^{-/-}$ MEFs than in WT MEFs (Figure 4G). When the exogenous Nrf2 was transiently expressed in 293T cells, in which the basal Nrf2 protein is hardly detected (Figure 5A, left panel), the cell number increase was significantly accelerated (Figure 5B), and the Nrf2 target genes were activated (Figure 5C). These effects were not observed when the mutant Nrf2 (Nrf2 CT) lacking the activation domain was expressed (Figures 5A, right panel, 5B and 5C). Thus, Nrf2 enhanced the proliferation of 293T cells, which depended on its transcriptional activation ability.

Since 293T cells turned out to display Nrf2-dependency in cell proliferation, we used 293T cells for analyzing the contribution of the PPP to proliferation as a downstream pathway of Nrf2. The cell number increase was significantly accelerated upon the expression of the exogenous G6PD or TKT (Figures 5D and 5E), indicating that selective increase of G6PD or TKT accelerated proliferation without activating the other Nrf2 target genes. Thus, the enhancement of the PPP activity accounts for the Nrf2-dependent cell proliferation at least in part.
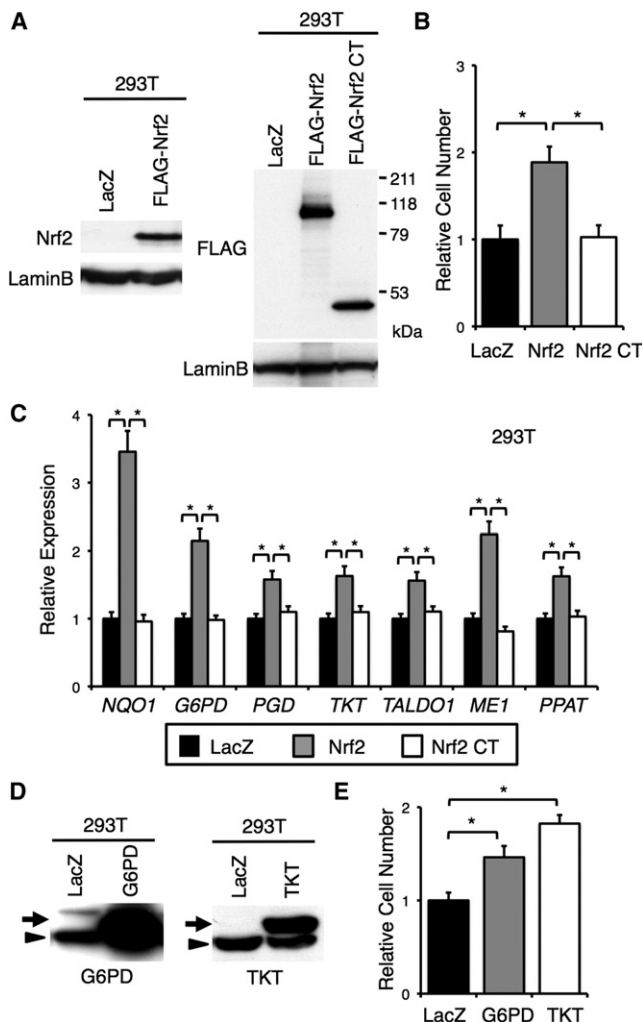
Figure 5. Increased Expression of Nrf2 or the PPP Enzymes Accelerates Cell Proliferation

(A) Immunoblot analysis of 293T cells expressing FLAG-Nrf2 and FLAG-Nrf2 CT. FLAG-Nrf2 was detected with anti-Nrf2 (left panel) and anti-FLAG (right panel) antibodies. LaminB was detected as a loading control.

(B) Effect of increased expression of Nrf2 on cell proliferation. FLAG-Nrf2 or FLAG-Nrf2 CT was expressed in 293T cells. Relative cell numbers are shown. The number of cells expressing LacZ was set to 1. Cells were counted at 96 hr after transfection.

(C) Gene expression in 293T cells transfected with an expression vector encoding LacZ, FLAG-Nrf2 or FLAG-Nrf2 CT. Cells were harvested at 48 hr after the transfection. Average values for cells expressing LacZ were set to 1.

(D) Immunoblot analysis of 293T cells expressing exogenous G6PD (left) and TKT (right). Arrowheads and arrows indicate endogenous and exogenous enzymes, respectively.

(E) Effect of increased expression of G6PD or TKT on cell proliferation. Relative cell numbers are shown. The number of cells expressing LacZ was set to 1. Cells were counted at 96 hr after transfection.

Average values and SDs were calculated from triplicate samples. *p < 0.01 (B, C and E).

Nrf2 Accumulation Promotes Cell Proliferation in the Forestomach Epithelium

Our next question was how Nrf2 contributes to the cell proliferation in normal cells in vivo. We utilized $Keap1^{F/-}$ mice as a source

of non-cancer cells with abundant Nrf2 protein (Taguchi et al., 2010). While the expression of $Nqo1$ was clearly higher in $Keap1^{F/-}$ mice in all the tissues examined, the metabolic genes were significantly activated in the forestomach and intestine but not in the liver (Figure 6A). These results suggest that Nrf2 induces the metabolic genes in the forestomach and intestine but does not do so efficiently in the liver. Comparison of $Nrf2^{-/-}$ and WT livers suggested that Nrf2 contributes to the basal expression rather than the inducible expression of the metabolic genes in the liver (Figure S4).

Because of the most marked induction of the metabolic genes by Keap1 reduction, we focused on the forestomach. Corresponding to the elevated gene expression, the enzyme protein levels were dramatically higher in the $Keap1^{F/-}$ forestomachs than the control samples (Figure 6B). The metabolic intermediates of glycolysis and the PPP were all decreased in the $Keap1^{F/-}$ forestomachs (Figure 6C). Hypoxanthine, xanthine and uric acid were all robustly increased in place of IMP (Figure 6C), implying that the excessive IMP may have been converted to uric acid (Figure 2A). These results were almost consistent with the metabolite pattern in $Keap1^{-/-}$ MEFs.

We then histologically examined the cell proliferation in the forestomach epithelia. In the $Keap1^{F/-}$ forestomach, the epithelial layer was hypertrophic, and abundant Nrf2 accumulation was clearly observed (Figure 6D). These results are consistent with those of our previous reports (Wakabayashi et al., 2003; Taguchi et al., 2010). The incorporation of BrdU was enhanced in the $Keap1^{F/-}$ forestomach (Figure 6D), suggesting that the accumulated Nrf2 provokes cell proliferation leading to the epithelial hypertrophy.

To validate the Nrf2-dependency of the phenotypes caused by the Keap1 reduction, we examined the forestomach epithelia in $Keap1^{-/-}::Nrf2^{-/-}$ mice. The expression of the metabolic genes in the forestomach was mostly comparable between $Nrf2^{-/-}$ and $Keap1^{-/-}::Nrf2^{-/-}$ mice (Figure 6E) and between WT and $Nrf2^{-/-}$ mice (Figure S4), indicating that $Keap1^{-/-}::Nrf2^{-/-}$ mice showed no or only marginal increase of the metabolic genes compared with WT mice. Neither epithelial hypertrophy nor enhanced incorporation of BrdU was seen in the $Keap1^{-/-}::Nrf2^{-/-}$ mice (Figure 6D). These results indicate that the accumulated Nrf2 is responsible for the phenotypes observed in $Keap1^{F/-}$ mice. Thus, Nrf2 activates metabolic genes, modulates the metabolite pattern and provokes cell proliferation when it accumulates in forestomach epithelial cells.

Nrf2 Enhances Metabolic Gene Expression in the Presence of Active PI3K-Akt Signaling

We were curious why Nrf2 accumulation had different effects on different tissues in terms of the metabolic gene activation (Figure 6A). Considering that epithelial tissues of the forestomach and intestine are composed of proliferating cells and that approximately 80% of the liver is composed of normally quiescent hepatocytes (Taub, 2004), we assumed that Nrf2 could effectively activate metabolic genes in the presence of proliferative signals.

The PI3K-Akt signaling pathway is one of the major contributors to cancer development because it promotes cancer cell growth, survival, and metabolism (Elstrom et al., 2004; Engelman, 2009). We compared the activities of the PI3K-Akt pathway
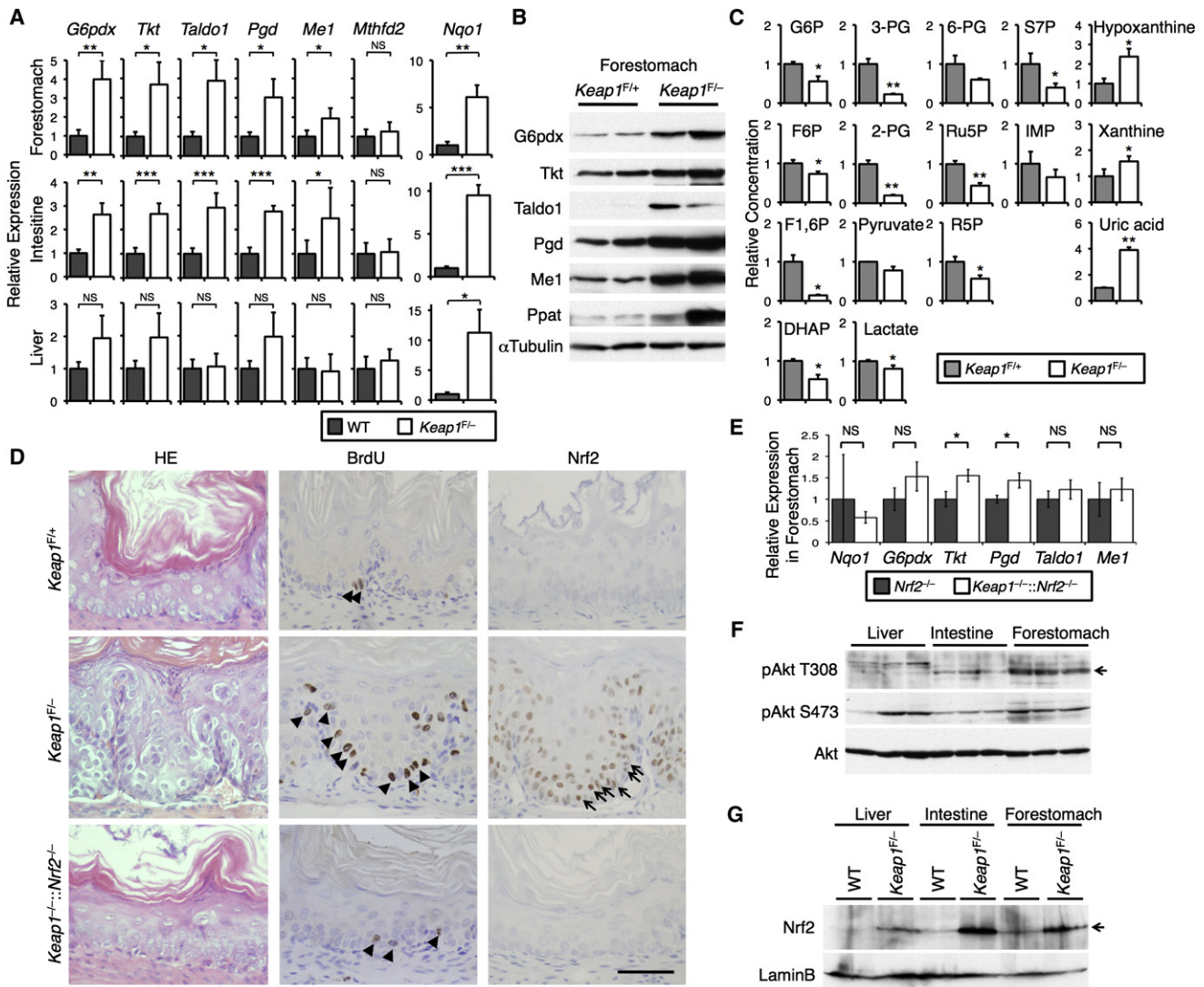
Figure 6. Effects of Nrf2 Accumulation in Forestomach Epithelia

(A) Gene expression in the forestomach, intestine and liver of WT (n = 6) and $Keap1^{F/-}$ (n = 4) mice. See also Figure S4.

(B) Immunoblot detection of the PPP and NADPH production enzymes in the forestomach epithelia of $Keap1^{F/+}$ and $Keap1^{F/-}$ mice. αTubulin was detected as a loading control.

(C) Quantification of metabolic intermediates of glycolysis and the PPP. IMP and its derivatives were also measured. Forestomach epithelia of $Keap1^{F/+}$ (n = 3) and $Keap1^{F/-}$ (n = 3) mice were analyzed.

(D) Histological analysis of the forestomach of $Keap1^{F/+}$ (n = 4), $Keap1^{F/-}$ (n = 4) and $Keap1^{-/-}::Nrf2^{-/-}$ (n = 3) mice. BrdU and Nrf2 were detected with specific antibodies (middle and right columns, respectively). Hematoxylin and eosin (HE) staining is shown in the left column. Representative micrographs are shown. A scale bar corresponds to 50 μm.

(E) Gene expression in the forestomach of $Nrf2^{-/-}$ (n = 3) and $Keap1^{-/-}::Nrf2^{-/-}$ (n = 3) mice.

(F) Phosphorylation of Akt in the forestomach, intestine, and liver of $Keap1^{F/-}$ mice. An arrow indicates the phosphorylated Akt at T308.

(G) Immunoblot analysis of Nrf2 in the forestomach, intestine and liver of WT and $Keap1^{F/-}$ mice. An arrow indicates Nrf2. LaminB was detected as a loading control.

Average values are shown, and error bars indicate SDs (A, C, and E). Average values for WT (A), $Keap1^{F/+}$ (C) or $Nrf2^{-/-}$ (E) were set to 1. *p < 0.05; **p < 0.01; ***p < 0.001 compared with WT (A), $Keap1^{F/+}$ (C) or $Nrf2^{-/-}$ (E).

in the $Keap1^{F/-}$ mouse tissues by monitoring the phosphorylation of Akt (Figure 6F). While the phosphorylation at S473 showed individual variability, the levels of T308 phosphorylation were markedly different among tissues; they were the highest in the forestomach, intermediate in the intestine, and almost undetectable in the liver. The phosphorylation at T308 is essential for the activation of Akt because T308 is positioned at the activation loop of the kinase (Casamayor et al., 1999). The Akt in the forestomach was likely to possess the highest activity. The cultured cells, including A549, 293, Jurkat, and MEFs, where Nrf2 activates the PPP, also showed the high levels of Akt phosphorylation at both sites (Figures 7A–7C and 7E). When the PI3K-Akt signaling was turned off by serum starvation, the highly expressed metabolic genes in $Keap1^{-/-}$ MEFs were decreased
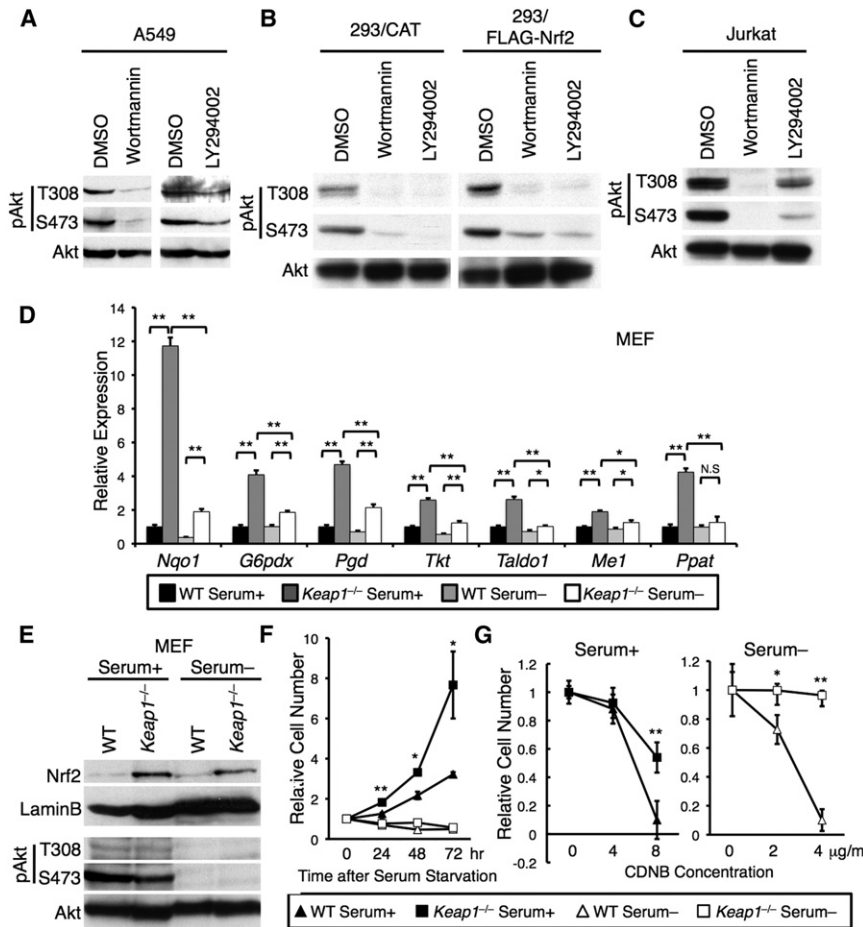
Figure 7. Nrf2 Enhances Metabolic Gene Expression in the Presence of Active PI3K-Akt Signaling in Cultured Cells

(A–C) Phosphorylation of Akt in cytoplasmic fractions of A549 cells (A), 293/CAT and 293/FLAG-Nrf2 cells (B), and Jurkat cells (C). Cells were treated with 5 μM Wortmannin (A–C) or LY294002 (20 μM for A and 50 μM for B and C) for 48 hr (A) and 3 hr (B and C).

(D) Gene expression in WT and $Keap1^{-/-}$ MEFs. Cells were cultured in the presence or absence of serum for 48 hr. Average values for the WT MEFs with serum were set to 1.

(E) Immunoblot analysis of Nrf2 and phosphorylated Akt in WT and $Keap1^{-/-}$ MEFs. Cells were cultured in the presence or absence of the serum for 48 hr. LaminB and total Akt were detected as loading controls.

(F) Cell number increase of WT and $Keap1^{-/-}$ MEFs cultured in the presence or absence of serum. The time was measured from the start of serum starvation. Initial cell numbers were set to 1.

(G) Susceptibility to CDNB treatment in WT and $Keap1^{-/-}$ MEFs under normal condition or serum starvation.

Average values and SDs were calculated from triplicate samples. *p < 0.05; **p < 0.001 (D, F and G).

closer to the WT levels (Figures 7D and 7E). Thus, we speculated that Nrf2 requires cooperation from active PI3K-Akt signaling to fully activate the metabolic genes.

It should be noted that both $Keap1^{-/-}$ and WT MEFs ceased proliferation under serum starvation, indicating that Nrf2 promotes cell proliferation only in the presence of proliferative signals (Figure 7F). In contrast, $Keap1^{-/-}$ MEFs were more resistant to the toxicity of 1-chloro-2,4-dinitrobenzene (CDNB) than WT MEFs with or without serum (Figure 7G), indicating that Nrf2 enhances cytoprotection irrespective of the activity of proliferative signals. These results implicate the functional expansion of Nrf2 in the presence of active PI3K-Akt signaling.

Forced Activation of PI3K Allows Nrf2 to Activate Metabolic Genes

To test this hypothesis, we activated the PI3K-Akt signaling pathway by deleting *Pten* in the liver and examined the gene expression (Figure 8A, left four bars). The livers of mice with four different genotypes were compared; $Pten^{F/F}$ (Control), $Pten^{F/F}$::*Alb*-Cre (*P-Alb*), $Keap1^{F/F}$::*Alb*-Cre (*K-Alb*) and $Pten^{F/F}$::$Keap1^{F/F}$::*Alb*-Cre (*P/K-Alb*). Because the *P/K-Alb* mice were lethal at approximately 3 weeks after birth due to unknown reasons, all the mice were examined on day 15 (P15). The *K-Alb* liver showed a modest increase in the metabolic gene expression but a robust increase in *Nqo1*, which is consistent

with the results observed in the $Keap1^{F/-}$ liver (Figure 6A). While the *P-Alb* liver showed only a slight increase in the expression of the genes examined, the *P/K-Alb* liver showed a marked increase in metabolic gene expression, even for *Mthfd2*, which was not elevated in $Keap1^{F/-}$ tissues (Figure 6A). A comparison of *P-Alb* and *P/K-Alb* showed that the *Keap1* deletion robustly increased the metabolic gene expression in addition to *Nqo1* in the absence of *Pten*, suggesting that the *Pten* deletion potentiates Nrf2 function and augments the induction of the ARE-driven genes by Nrf2.

To verify the contribution of Nrf2 to the expression of the metabolic genes, we examined the livers of mice in the *Nrf2* null background; $Pten^{F/F}$::$Nrf2^{-/-}$ (Nrf2-KO), $Pten^{F/F}$::*Alb*-Cre::$Nrf2^{-/-}$ (*P-Alb/N*), $Pten^{F/F}$::$Keap1^{F/F}$::*Alb*-Cre::$Nrf2^{-/-}$ (*P/K-Alb/N*), and $Pten^{F/F}$::$Keap1^{F/F}$::*Alb*-Cre::$Nrf2^{+/-}$ (*P/K-Alb/N*-h) (Figure 8A, right four bars). The gene expression in the *P/K-Alb/N* liver was much lower than that in the *P/K-Alb* liver and as low as that in the *P-Alb* liver, indicating that Nrf2 is essential for the marked elevation of the gene expression in the *P/K-Alb* liver. The expression levels of *Me1* and *Nqo1* of the *P/K-Alb/N*-h liver were intermediate between the *P/K-Alb* and *P/K-Alb/N* livers. The expression of the rest of the genes in the *P/K-Alb/N*-h liver was as low as that observed in the *P/K-Alb/N* liver. These results indicate that the transcriptional activation of the metabolic genes requires higher Nrf2 activity than the cytoprotective genes.

We further examined the effect of active PI3K-Akt signaling on the Nrf2 function to modulate the metabolic activity in the liver. The metabolic intermediates were measured in the livers of Control, *P-Alb*, *K-Alb*, *P/K-Alb* and *P/K-Alb/N* mice using CE-MS (Figure 8B). The abundance of PPP intermediates, IMP and
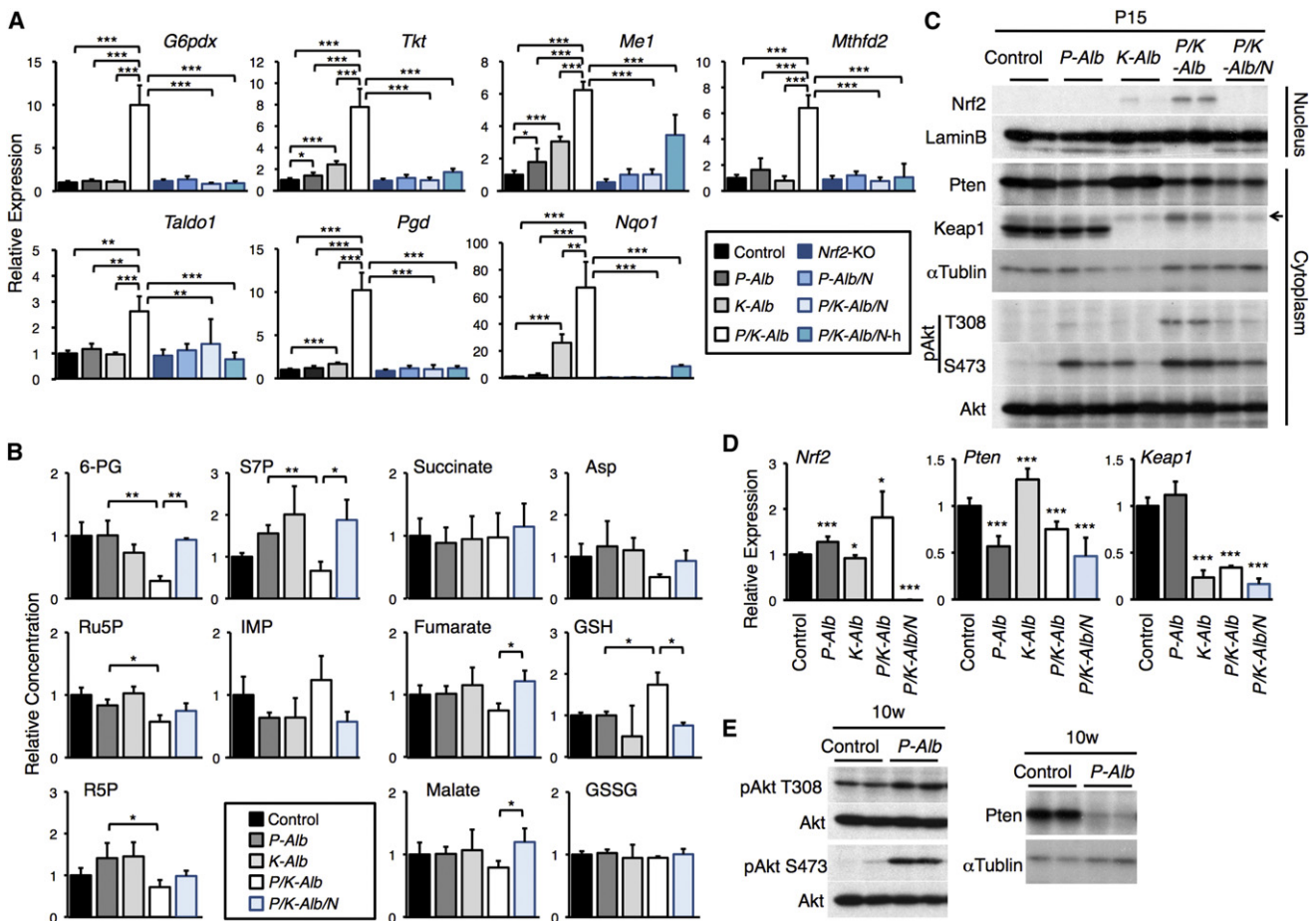
Figure 8. Forced Activation of PI3K-Akt Signaling in the Liver Enhances Nrf2 Activity

(A) Gene expression in the liver of Control (n = 3), *P-Alb* (n = 4), *K-Alb* (n = 4), *P/K-Alb* (n = 3), *Nrf2*-KO (n = 6), *P-Alb/N* (n = 5), *P/K-Alb/N* (n = 4), and *P/K-Alb/N*-h (n = 4) mice.

(B) Quantification of the intermediates of the PPP and glutamine metabolism and IMP in the liver of Control (n = 3), *P-Alb* (n = 3), *K-Alb* (n = 3), *P/K-Alb* (n = 3), and *P/K-Alb/N* (n = 3) mice.

(C) Immunoblot detection of Nrf2, Pten, Keap1, and phosphorylated Akt in the liver of Control, *P-Alb*, *K-Alb*, *P/K-Alb* and *P/K-Alb/N* mice at P15. LaminB and αTubulin were detected as loading controls.

(D) mRNA expression of *Nrf2*, *Pten*, and *Keap1* in the liver of Control (n = 3), *P-Alb* (n = 4), *K-Alb* (n = 4), *P/K-Alb* (n = 3), and *P/K-Alb/N* (n = 4) mice.

(E) Immunoblot detection of Pten and phosphorylated Akt in the livers of Control and *P-Alb* mice at 10 weeks. αTubulin was detected as a loading control.

Average values are shown, and error bars indicate SDs. Average values for Control samples were set to 1 (A, B, and D). *p < 0.05; **p < 0.01; ***p < 0.001 (compared with Control in panel D).

GSH were almost comparable between Control and *K-Alb* livers, suggesting that simple Nrf2 accumulation does not alter the metabolite pattern. Importantly, the PPP intermediates were significantly lower in *P/K-Alb* liver than in *P-Alb* liver, and the decrease was restored in *P/K-Alb/N* liver. IMP tended to be higher in *P/K-Alb* than *P-Alb*, and the increase was not observed in *P/K-Alb/N*. Similarly, GSH was significantly higher in *P/K-Alb* than *P-Alb*, and the increase was canceled in *P/K-Alb/N*. These results implied that Nrf2 accumulation affects the metabolite pattern in the presence of active PI3K-Akt pathway.

Forced Activation of PI3K Enhances the Nuclear Availability of Nrf2

To elucidate the underlying mechanisms of the functional potentiation of Nrf2, we examined the protein abundance of Nrf2 in liver nuclear extracts (Figure 8C). Whereas *K-Alb* liver showed slight increases in Nrf2 compared with the Control and *P-Alb* livers, nuclear extracts from the *P/K-Alb* liver contained dramatically increased Nrf2. We also found that *Nrf2* mRNA was more abundant in the *P/K-Alb* liver compared with the rest of the mice, suggesting the increased production of Nrf2 in the *P/K-Alb* liver (Figure 8D). Thus, the quantitative increase in nuclear Nrf2 is regarded to be the primary cause of the elevated expression of Nrf2 target genes in the *P/K-Alb* mice. Importantly, Keap1 protein was barely detectable in either the *K-Alb* or *P/K-Alb* livers (Figure 8C), which indicates that the enhanced nuclear accumulation of Nrf2 is independent of Keap1 deficiency but dependent on the disruption of the *Pten* gene. Consistently, the Nrf2 protein was more abundant in the tissues and cells with higher activity of PI3K-Akt signaling; the forestomach and intestine accumulates

more Nrf2 than the liver in *Keap1*^{F/−} mice (Figure 6G), and *Keap1*^{−/−} MEFs with serum accumulates more Nrf2 than those without serum (Figure 7E).

We then examined the phosphorylation of Akt, which was present at low levels in the *P-Alb* liver at P15 (Figure 8C) but was markedly increased at 10 weeks (Figure 8E, left panel). Considering the postnatal expression of Cre recombinase driven by the albumin promoter, the *Pten* gene was not fully disrupted at P15, and *Pten* mRNA was present in the *P-Alb*, *P/K-Alb*, and *P/K-Alb/N* livers by 50% of the control liver (Figure 8D). Accordingly, the *P-Alb*, *P/K-Alb*, and *P/K-Alb/N* livers at P15 showed approximately 50% reduction of the Pten protein compared with that in the control liver (Figure 8C), whereas it was hardly detected in the 10-week-old *Pten-Alb* liver (Figure 8E, right panel). Despite the partial depletion of Pten, Akt phosphorylation, especially at T308, was markedly enhanced in the *P/K-Alb* liver but not in the *P-Alb* liver (Figure 8C). Therefore, the augmented Akt phosphorylation is independent of Pten reduction but is attributed to the disruption of the *Keap1* gene. The enhancement of Akt phosphorylation in the *P/K-Alb* liver was absent in the *P/K-Alb/N* liver, which indicates that accumulated Nrf2 is responsible for the increased phosphorylation of Akt. Nrf2 accumulation may have augmented the Akt phosphorylation in the *Keap1*^{F/−} forestomach and intestine (Figure 6F). Thus, the activation of the PI3K-Akt pathway enhances Nrf2 activity by increasing its nuclear availability, and the activated Nrf2 in turn promotes the further activation of the PI3K-Akt pathway. This positive feedback is one of the molecular mechanisms underlying the aggravating role of Nrf2 in cancer progression.

DISCUSSION

This study demonstrated a contribution of Nrf2 to cellular metabolic activities in proliferating cells. While being a key regulator of redox homeostasis in quiescent cells, Nrf2 activates the metabolic genes in addition to the cytoprotective genes in proliferating cells, which is advantageous for proliferation and survival. Metabolomic profilings revealed that Nrf2 promotes the purine nucleotide synthesis and glutamine metabolism in the presence of active PI3K-Akt signaling.

We identified six genes involved in the PPP and NADPH production pathways as direct targets of Nrf2. Some of these genes were listed as Nrf2 targets in previous microarray analyses conducted in mouse and human (Thimmulappa et al., 2002; MacLeod et al., 2009). These genes, except for *Me1*, were also listed as direct target genes of Nrf2 in an earlier ChIP-seq analysis with anti-Nrf2 antibody using MEFs (Malhotra et al., 2010). While a previous study focused on a cytoprotective aspect of the PPP by analyzing the NADPH production as reducing equivalents for the ROS elimination (Wu et al., 2011), this study showed that the increase of the PPP activity accounts for the Nrf2-dependent proliferation. We further identified the PI3K-Akt pathway as one of the proliferative signals augmenting Nrf2-dependent transcription. Since the PPP genes are strongly activated by Nrf2 in proliferating cells in which PI3K-Akt pathway is active, it is pertinent that the increased expression of the PPP genes contributes to cell proliferation.

In addition to the PPP, or the pre-R5P steps of the nucleotide synthesis, our metabolomic profilings revealed that Nrf2 strongly enhances the latter part of the nucleotide synthesis, or the post-R5P steps. Although we currently do not know the molecular mechanisms how Nrf2 promotes the post-R5P steps, we speculate that the functional enhancement of Ppat and Mthfd2 is one of the regulatory targets of Nrf2 (see Figures 1B, 4D, 6B, and 8A). Nrf2 may also promote the glutamine-utilizing reactions in the post-R5P steps, which could partly explain the glutamine consumption mediated by Nrf2. We surmise that the post-transcriptional regulation of key enzymes catalyzing the reactions in the post-R5P steps explains the discordance between the Nrf2-dependent transcriptome and metabolome. In addition, Nrf2 may indirectly promote the synthesis of 10-formyl-tetrahydrofolate (THF), which is an important substrate in post-R5P steps, though supplying NADPH for the THF production. With these possibilities, Nrf2 directly and/or indirectly controls the complex multilayered regulation of the post-R5P steps.

The importance of glutathione has been recognized from the viewpoint of the detoxification of xenobiotics and ROS. However, recent studies have revealed that glutathione is critical for cell proliferation (Reddy et al., 2007; 2008; Ishimoto et al., 2011). Intriguingly, glutathione could not be replaced with N-acetylcysteine for the proliferation-promoting activity, suggesting that glutathione does more than simply correct the redox balance to fully support cell proliferation (Reddy et al., 2008). The metabolomic profiling showed that a substantial amount of glutamine is directed into glutathione synthesis, to which Nrf2 makes a large contribution. Nrf2 induces GCL, a key enzyme for glutathione synthesis, by directly activating the genes encoding the catalytic and regulatory subunits, *GCL catalytic subunit* (*GCLC*) and *GCL modifier subunit* (*GCLM*) (Moinova and Mulcahy, 1999; Solis et al., 2002; Bea et al., 2003; Sekhar et al., 2003). Nrf2 also increases the supply of cysteine by directly activating the gene encoding xCT (*SLC7A11*), a subunit of the cystine transporter (Sasaki et al., 2002). Because Nrf2 strongly activates *Gclc*, *Gclm*, and *Slc7a11* in the presence of active PI3K-Akt signaling (K.T., unpublished data), the enhancement of glutathione synthesis is an important downstream of Nrf2 in accelerating proliferation.

The functional interaction between the Keap1-Nrf2 pathway and Pten-PI3K-Akt pathway has been reported in several studies using cell lines. The pharmacological inhibition of the PI3K-Akt pathway represses the nuclear translocation of Nrf2 (Harrison et al., 2006; So et al., 2006). Consistent with these reports, we have shown that activation of the PI3K-Akt pathway increases the abundance of nuclear Nrf2. Recently GSK-3 was shown to promote Keap1-independent degradation of Nrf2 (Rada et al., 2011). Because Akt phosphorylates GSK-3 and inhibits its activity (Cross et al., 1995), the active PI3K-Akt signaling should stabilize Nrf2 through repressing GSK-3.

Unexpectedly, Akt phosphorylation was robustly augmented in the *P/K-Alb* mice in Nrf2-dependent manner, which is consistent with the previous report that Nrf2 positively regulates the activation of Akt (Beyer et al., 2008). Considering that SREBP has been suggested to induce the PPP genes when mTORC1 is activated (Düvel et al., 2010), Nrf2 could indirectly activate the PPP through the Akt-mTORC1-SREBP axis in addition to its role in the direct regulation of the PPP.

The genetic inactivation of PTEN leading to the constitutive activation of PI3K-Akt signaling has been identified in many

human cancers (Li et al., 1997). Many oncogenic signals also activate the PI3K-Akt signaling pathway (Yuan and Cantley, 2008). This study demonstrated the positive feedback loop between the Pten-PI3K-Akt and Keap1-Nrf2 pathways, which appears to be one of the most substantial mechanisms for promoting the malignant evolution of cancers. Efficient cancelation of the feedback would be an effective strategy for anti-cancer therapy. It should be noted that a high level of Nrf2 accumulation, which is achieved by the functional impairment of Keap1 combined with the sustained activation of PI3K-Akt pathway, allows Nrf2 to get involved in the modulation of metabolism under pathological conditions. In contrast, temporary accumulation of Nrf2 at a low level is sufficient for Nrf2 to exert the cytoprotective function under physiological conditions. The marked difference in Nrf2 activities between cancers and normal tissues may provide a clue to the selective inhibition of Nrf2 in cancers.

EXPERIMENTAL PROCEDURES

Cell Culture
Two cell lines with *KEAP1* mutations (A549 and H2126) and two cell lines with *NRF2* mutations (LK2 and EBC1) were used. 293/CAT cells and 293/FALG-Nrf2 cells were established previously (Zhang et al., 2007). MEFs were established from *Keap1$^{-/-}$* and WT mouse embryos (Wakabayashi et al., 2003).

Microarray Analysis
Total RNA from A549 cells was labeled with Cy3. Samples were hybridized to the Human Oligo Microarray (Agilent) according to the manufacturer's protocol. Arrays were scanned using the G2539A Microarray Scanner system (Agilent), and the resulting data were analyzed using GeneSpring GX software (Agilent).

Tumor Xenograft Experiment
A549 cells were subcutaneously injected into the upper back region of eight-week-old male nude mice (BALB/C nu/nu). Tumor size was measured every three days using calipers.

Animals
The generation of *Nrf2$^{+/-}$*, *Keap1$^{+/-}$*, *Keap1$^{F/+}$*, and *Pten$^{F/+}$* mice has been described (Itoh et al., 1997; Wakabayashi et al., 2003; Okawa et al., 2006; Horie et al., 2004). *Pten$^{F/+}$* mice were a kind gift from Dr. Akira Suzuki (Kyushu University). *Alb*-Cre transgenic mice were purchased from Jackson Laboratory. All mice were kept under specific pathogen-free conditions and treated according to the regulations presented in The Standards for Human Care and Use of Laboratory Animals of Tohoku University and Guidelines for Proper Conduct of Animal Experiments by the Ministry of Education, Culture, Sports, Science, and Technology of Japan. All the animal experiments were approved at The Tohoku University Committee for Laboratory Animal Research.

Cell Viability Assay
MEFs were seeded at the initial density of 1×10^4 cells/well in 96-well plates and cultured for 24 hr in the presence of 10% FBS or in the absence of FBS. Cells were then treated with 1-chloro-2,4-dinitrobenzene (CDNB; WAKO Pure Chemicals). After 12 hr of culturing, viable cell numbers were quantified with the Cell Counting Kit-8 (Dojindo Molecular Technologies, Inc.) according to the manufacturer's protocol.

BrdU Assay
BrdU was intraperitoneally injected into mice at the dose of 100 mg/kg body weight. One hour after the injection, mice were sacrificed and analyzed using BrdU Immunohistochemistry System (Merck Calbiochem).

Metabolite Measurements
Extracts were prepared from 2 to 6×10^6 cells or approximately 50 mg of tissues with methanol containing Internal Standard Solution (Human Metabo-

lime Technoligies) and analyzed using a capillary electrophoresis (CE)-connected ESI-TOFMS system.

Statistical Analyses
All differences were analyzed with Student's t test. A p value less than 0.05 was considered to be statistically significant.

REFERENCES

Bea, F., Hudson, F.N., Chait, A., Kavanagh, T.J., and Rosenfeld, M.E. (2003). Induction of glutathione synthesis in macrophages by oxidized low-density lipoproteins is mediated by consensus antioxidant response elements. Circ. Res. *92*, 386–393.

Bensaad, K., Tsuruta, A., Selak, M.A., Vidal, M.N., Nakano, K., Bartrons, R., Gottlieb, E., and Vousden, K.H. (2006). TIGAR, a p53-inducible regulator of glycolysis and apoptosis. Cell *126*, 107–120.

Beyer, T.A., Xu, W., Teupser, D., auf dem Keller, U., Bugnon, P., Hildt, E., Thiery, J., Kan, Y.W., and Werner, S. (2008). Impaired liver regeneration in Nrf2 knockout mice: role of ROS-mediated insulin/IGF-1 resistance. EMBO J. *27*, 212–223.

Casamayor, A., Morrice, N.A., and Alessi, D.R. (1999). Phosphorylation of Ser-241 is essential for the activity of 3-phosphoinositide-dependent protein kinase-1: identification of five sites of phosphorylation in vivo. Biochem. J. *342*, 287–292.

Cross, D.A.E., Alessi, D.R., Cohen, P., Andjelkovich, M., and Hemmings, B.A. (1995). Inhibition of glycogen synthase kinase-3 by insulin mediated by protein kinase B. Nature *378*, 785–789.

Dang, C.V. (2010). Glutaminolysis: supplying carbon or nitrogen or both for cancer cells? Cell Cycle *9*, 3884–3886.

DeBerardinis, R.J., Mancuso, A., Daikhin, E., Nissim, I., Yudkoff, M., Wehrli, S., and Thompson, C.B. (2007). Beyond aerobic glycolysis: transformed cells can engage in glutamine metabolism that exceeds the requirement for protein and nucleotide synthesis. Proc. Natl. Acad. Sci. USA *104*, 19345–19350.

DeBerardinis, R.J., Lum, J.J., Hatzivassiliou, G., and Thompson, C.B. (2008). The biology of cancer: metabolic reprogramming fuels cell growth and proliferation. Cell Metab. *7*, 11–20.

Düvel, K., Yecies, J.L., Menon, S., Raman, P., Lipovsky, A.I., Souza, A.L., Triantafellow, E., Ma, Q., Gorski, R., Cleaver, S., et al. (2010). Activation of a metabolic gene regulatory network downstream of mTOR complex 1. Mol. Cell 39, 171–183.

Elstrom, R.L., Bauer, D.E., Buzzai, M., Karnauskas, R., Harris, M.H., Plas, D.R., Zhuang, H., Cinalli, R.M., Alavi, A., Rudin, C.M., and Thompson, C.B. (2004). Akt stimulates aerobic glycolysis in cancer cells. Cancer Res. 64, 3892–3899.

Engelman, J.A. (2009). Targeting PI3K signalling in cancer: opportunities, challenges and limitations. Nat. Rev. Cancer 9, 550–562.

Harrison, E.M., McNally, S.J., Devey, L., Garden, O.J., Ross, J.A., and Wigmore, S.J. (2006). Insulin induces heme oxygenase-1 through the phosphatidylinositol 3-kinase/Akt pathway and the Nrf2 transcription factor in renal cells. FEBS J. 273, 2345–2356.

Horie, Y., Suzuki, A., Kataoka, E., Sasaki, T., Hamada, K., Sasaki, J., Mizuno, K., Hasegawa, G., Kishimoto, H., Iizuka, M., et al. (2004). Hepatocyte-specific Pten deficiency results in steatohepatitis and hepatocellular carcinomas. J. Clin. Invest. 113, 1774–1783.

Ishimoto, T., Nagano, O., Yae, T., Tamada, M., Motohara, T., Oshima, H., Oshima, M., Ikeda, T., Asaba, R., Yagi, H., et al. (2011). CD44 variant regulates redox status in cancer cells by stabilizing the xCT subunit of system xc(-) and thereby promotes tumor growth. Cancer Cell 19, 387–400.

Itoh, K., Chiba, T., Takahashi, S., Ishii, T., Igarashi, K., Katoh, Y., Oyake, T., Hayashi, N., Satoh, K., Hatayama, I., et al. (1997). An Nrf2/small Maf heterodimer mediates the induction of phase II detoxifying enzyme genes through antioxidant response elements. Biochem. Biophys. Res. Commun. 236, 313–322.

Kim, Y.R., Oh, J.E., Kim, M.S., Kang, M.R., Park, S.W., Han, J.Y., Eom, H.S., Yoo, N.J., and Lee, S.H. (2010). Oncogenic NRF2 mutations in squamous cell carcinomas of oesophagus and skin. J. Pathol. 220, 446–451.

Kroemer, G., and Pouyssegur, J. (2008). Tumor cell metabolism: cancer's Achilles' heel. Cancer Cell 13, 472–482.

Li, J., Yen, C., Liaw, D., Podsypanina, K., Bose, S., Wang, S.I., Puc, J., Miliaresis, C., Rodgers, L., McCombie, R., et al. (1997). PTEN, a putative protein tyrosine phosphatase gene mutated in human brain, breast, and prostate cancer. Science 275, 1943–1947.

Lu, S.C. (2009). Regulation of glutathione synthesis. Mol. Aspects Med. 30, 42–59.

MacLeod, A.K., McMahon, M., Plummer, S.M., Higgins, L.G., Penning, T.M., Igarashi, K., and Hayes, J.D. (2009). Characterization of the cancer chemopreventive NRF2-dependent gene battery in human keratinocytes: demonstration that the KEAP1-NRF2 pathway, and not the BACH1-NRF2 pathway, controls cytoprotection against electrophiles as well as redox-cycling compounds. Carcinogenesis 30, 1571–1580.

Malhotra, D., Portales-Casamar, E., Singh, A., Srivastava, S., Arenillas, D., Happel, C., Shyr, C., Wakabayashi, N., Kensler, T.W., Wasserman, W.W., and Biswal, S. (2010). Global mapping of binding sites for Nrf2 identifies novel targets in cell survival response through ChIP-Seq profiling and network analysis. Nucleic Acids Res. 38, 5718–5734.

Moinova, H.R., and Mulcahy, R.T. (1999). Up-regulation of the human gamma-glutamylcysteine synthetase regulatory subunit gene involves binding of Nrf-2 to an electrophile responsive element. Biochem. Biophys. Res. Commun. 261, 661–668.

Okawa, H., Motohashi, H., Kobayashi, A., Aburatani, H., Kensler, T.W., and Yamamoto, M. (2006). Hepatocyte-specific deletion of the keap1 gene activates Nrf2 and confers potent resistance against acute drug toxicity. Biochem. Biophys. Res. Commun. 339, 79–88.

Rada, P., Rojo, A.I., Chowdhry, S., McMahon, M., Hayes, J.D., and Cuadrado, A. (2011). SCF/beta-TrCP promotes glycogen synthase kinase 3-dependent degradation of the Nrf2 transcription factor in a Keap1-independent manner. Mol. Cell. Biol. 31, 1121–1133.

Reddy, N.M., Kleeberger, S.R., Cho, H.Y., Yamamoto, M., Kensler, T.W., Biswal, S., and Reddy, S.P. (2007). Deficiency in Nrf2-GSH signaling impairs type II cell growth and enhances sensitivity to oxidants. Am. J. Respir. Cell Mol. Biol. 37, 3–8.

Reddy, N.M., Kleeberger, S.R., Bream, J.H., Fallon, P.G., Kensler, T.W., Yamamoto, M., and Reddy, S.P. (2008). Genetic disruption of the Nrf2 compromises cell-cycle progression by impairing GSH-induced redox signaling. Oncogene 27, 5821–5832.

Sakamoto, K., Iwasaki, K., Sugiyama, H., and Tsuji, Y. (2009). Role of the tumor suppressor PTEN in antioxidant responsive element-mediated transcription and associated histone modifications. Mol. Biol. Cell 20, 1606–1617.

Sasaki, H., Sato, H., Kuriyama-Matsumura, K., Sato, K., Maebara, K., Wang, H., Tamba, M., Itoh, K., Yamamoto, M., and Bannai, S. (2002). Electrophile response element-mediated induction of the cystine/glutamate exchange transporter gene expression. J. Biol. Chem. 277, 44765–44771.

Sekhar, K.R., Crooks, P.A., Sonar, V.N., Friedman, D.B., Chan, J.Y., Meredith, M.J., Starnes, J.H., Kelton, K.R., Summar, S.R., Sasi, S., and Freeman, M.L. (2003). NADPH oxidase activity is essential for Keap1/Nrf2-mediated induction of GCLC in response to 2-indol-3-yl-methylenequinuclidin-3-ols. Cancer Res. 63, 5636–5645.

Shibata, T., Ohta, T., Tong, K.I., Kokubu, A., Odogawa, R., Tsuta, K., Asamura, H., Yamamoto, M., and Hirohashi, S. (2008). Cancer related mutations in NRF2 impair its recognition by Keap1-Cul3 E3 ligase and promote malignancy. Proc. Natl. Acad. Sci. USA 105, 13568–13573.

Singh, A., Misra, V., Thimmulappa, R.K., Lee, H., Ames, S., Hoque, M.O., Herman, J.G., Baylin, S.B., Sidransky, D., Gabrielson, E., et al. (2006). Dysfunctional KEAP1-NRF2 interaction in non-small-cell lung cancer. PLoS Med. 3, e420.

Singh, A., Boldin-Adamsky, S., Thimmulappa, R.K., Rath, S.K., Ashush, H., Coulter, J., Blackford, A., Goodman, S.N., Bunz, F., Watson, W.H., et al. (2008). RNAi-mediated silencing of nuclear factor erythroid-2-related factor 2 gene expression in non-small cell lung cancer inhibits tumor growth and increases efficacy of chemotherapy. Cancer Res. 68, 7975–7984.

So, H.S., Kim, H.J., Lee, J.H., Lee, J.H., Park, S.Y., Park, C., Kim, Y.H., Kim, J.K., Lee, K.M., Kim, K.S., et al. (2006). Flunarizine induces Nrf2-mediated transcriptional activation of heme oxygenase-1 in protection of auditory cells from cisplatin. Cell Death Differ. 13, 1763–1775.

Solis, W.A., Dalton, T.P., Dieter, M.Z., Freshwater, S., Harrer, J.M., He, L., Shertzer, H.G., and Nebert, D.W. (2002). Glutamate-cysteine ligase modifier subunit: mouse Gclm gene structure and regulation by agents that cause oxidative stress. Biochem. Pharmacol. 63, 1739–1754.

Solis, L.M., Behrens, C., Dong, W., Suraokar, M., Ozburn, N.C., Moran, C.A., Corvalan, A.H., Biswal, S., Swisher, S.G., Bekele, B.N., et al. (2010). Nrf2 and Keap1 abnormalities in non-small cell lung carcinoma and association with clinicopathologic features. Clin. Cancer Res. 16, 3743–3753.

Taguchi, K., Shimada, M., Fujii, S., Sumi, D., Pan, X., Yamano, S., Nishiyama, T., Hiratsuka, A., Yamamoto, M., Cho, A.K., et al. (2008). Redox cycling of 9,10-phenanthraquinone to cause oxidative stress is terminated through its monoglucuronide conjugation in human pulmonary epithelial A549 cells. Free Radic. Biol. Med. 44, 1645–1655.

Taguchi, K., Maher, J.M., Suzuki, T., Kawatani, Y., Motohashi, H., and Yamamoto, M. (2010). Genetic analysis of cytoprotective functions supported by graded expression of Keap1. Mol. Cell. Biol. 30, 3016–3026.

Taub, R. (2004). Liver regeneration: from myth to mechanism. Nat. Rev. Mol. Cell Biol. 5, 836–847.

Thimmulappa, R.K., Mai, K.H., Srisuma, S., Kensler, T.W., Yamamoto, M., and Biswal, S. (2002). Identification of Nrf2-regulated genes induced by the chemopreventive agent sulforaphane by oligonucleotide microarray. Cancer Res. 62, 5196–5203.

Tong, X., Zhao, F., and Thompson, C.B. (2009). The molecular determinants of de novo nucleotide biosynthesis in cancer cells. Curr. Opin. Genet. Dev. 19, 32–37.

Uruno, A., and Motohashi, H. (2011). The Keap1-Nrf2 system as an in vivo sensor for electrophiles. Nitric Oxide 25, 153–160.

Wakabayashi, N., Itoh, K., Wakabayashi, J., Motohashi, H., Noda, S., Takahashi, S., Imakado, S., Kotsuji, T., Otsuka, F., Roop, D.R., et al. (2003). Keap1-null mutation leads to postnatal lethality due to constitutive Nrf2 activation. Nat. Genet. 35, 238–245.

Wang, R., An, J., Ji, F., Jiao, H., Sun, H., and Zhou, D. (2008). Hypermethylation of the Keap1 gene in human lung cancer cell lines and lung cancer tissues. Biochem. Biophys. Res. Commun. *373*, 151–154.

Wu, K.C., Cui, J.Y., and Klaassen, C.D. (2011). Beneficial role of Nrf2 in regulating NADPH generation and consumption. Toxicol. Sci. *123*, 590–600.

Yuan, T.L., and Cantley, L.C. (2008). PI3K pathway alterations in cancer: variations on a theme. Oncogene *27*, 5497–5510.

Zhang, J., Hosoya, T., Maruyama, A., Nishikawa, K., Maher, J.M., Ohta, T., Motohashi, H., Fukamizu, A., Shibahara, S., Itoh, K., and Yamamoto, M. (2007). Nrf2 Neh5 domain is differentially utilized in the transactivation of cytoprotective genes. Biochem. J. *404*, 459–466.

Zhang, P., Singh, A., Yegnasubramanian, S., Esopi, D., Kombairaju, P., Bodas, M., Wu, H., Bova, S.G., and Biswal, S. (2010). Loss of Kelch-like ECH-associated protein 1 function in prostate cancer cells causes chemoresistance and radioresistance and promotes tumor growth. Mol. Cancer Ther. *9*, 336–346.